Modeling Cardiac Mechanics of Left Ventricular NonCompaction

Journal:	*Computer Methods in Biomechanics and Biomedical Engineering: Imaging & Visualization*
Manuscript ID	TCIV-2020-0053.R2
Manuscript Type:	Research Manuscripts
Date Submitted by the Author:	n/a
Complete List of Authors:	rinaudo, antonino; University of Palermo scardulla, francesco; University of Palermo d'acquisto, leonardo; University of Palermo scardulla, cesare; ISMETT pasta, salvatore; University of Palermo,
Keywords:	left ventricular noncompaction, Computational Bio- imaging and Visualization

Modeling Cardiac Mechanics of Left Ventricular NonCompaction

Antonino Rinaudo[1], PhD, Francesco Scardulla[1],PhD,
Leonardo D'Acquisto[1], PhD Cesare Scardulla[2], MD, Salvatore Pasta[1*], PhD (0000-0002-4841-2560)

[1] Department of Engineering, University of Palermo, viale delle Scienze, Ed.8, 90128, Palermo, Italy,

[2] Department for the Treatment and Study of Cardiothoracic Diseases and Cardiothoracic Transplantation, IRCCS-ISMETT, via Tricomi n.5, 90127, Palermo, Italy

Word count:4331

Funding: this work was supported by the Italian Ministry of Health under grant GR-2011-02348129

Disclosure statement: none

[*] Corresponding author:
Salvatore Pasta, PhD
Professor of Industrial Bioengineering,
Department of Engineering
University of Palermo
Phone: +39 091 3815681
FAX: +39 091 3815682
e-mail: salvatore.pasta@unipa.it

ABSTRACT

Left ventricular noncompaction (LVNC) can be defined as a cardiomyopathy characterized by a pattern of prominent trabecular structure and deep intertrabecular recesses, that is thought to be caused by an arrest of normal endomyocardial morphogenesis. Using patient-specific computational modeling, we assessed the cardiac mechanics of five patients with LVNC and compared myocardial stress and pump performance to those of healthy controls. Findings shown that patients with LVNC have impaired left ventricular (LV) function, making it possible that the lack of fiber shortening of noncompacted layer can determine poor heart function. Pronounced end-systolic wall stress on left ventricular wall of patients with LVNC was observed when compared to that of normal hearts, and this may lead to adverse cardiac remodeling and ultimately heart failure. We hereby suggest that computational modeling can be considered as a useful tool to assess the cardiac work and pump performance of LVNC, which are responsible for progressive left ventricular deterioration and poor clinical course.

Keywords: left ventricular noncompaction; finite element analysis, wall stress, cardiac mechanics

INTRODUCTION

Left ventricular noncompaction (LVNC) is a relatively cardiomyopathy characterized by an arrest in the normal process of myocardial morphogenesis, resulting in excessive and prominent trabeculations of muscle fiber mesh and deep endomyocardial spaces (Ichida 2009; Sarma et al. 2010). Increased trabeculation and deep intertrabecular recesses communicate with the left ventricular (LV) cavity. The functional consequence of LVNC is a reduced efficiency of the normal left ventricular (LV) twist and depressed pump performance, which lead ultimately to early heart failure. The diagnosis and management of patients with LVNC is crucial as the clinical manifestation induces to relevant morbidity and mortality caused by early heart failure, life threatening ventricular arrhythmias and systemic embolic events (Jenni et al. 2001; van Dalen et al. 2011).

Mathematical modeling of the cardiovascular system using finite element (FE) analysis is an useful tool to estimate the cardiac mechanics and wall stress, likely inhibiting the function of LVNC (Lee et al. 2014). Several FE modeling studies of the LV have been presented for cardiomyopathy (Quarterman et al. 2002; Zhong et al. 2009; Scardulla et al. 2016), pericardial effusion (Scardulla et al. 2015), left ventricular assist device (Sack et al. 2018; Scardulla, Agnese, et al. 2018), right heart failure induced by pulmonary hypertension (Scardulla, Bellavia, et al. 2018). Guccione et al. (Guccione et al. 2001) have successfully modeled end-isovolumic systole in an ovine model of myocardial infarction and determined material parameters that reproduced circumferential stretching (as measured with 2D tagged MRI) in the infarcted border zone. The key role of wall stress in the progression of LV remodeling was studied in dilated cardiomyopathy (Ratcliffe et al. 1998; Quarterman et al. 2002; Zhong et al. 2009). Lee et al. (Lee et al. 2014) demonstrated the main advantage of the FE method over Laplace's law to assess cardiac mechanics. An increase in wall stress is known to reduce myocardial fiber

shortening, and increases myocardial stress. LV wall stress is in part determined by geometric features of LV so that trabeculations induced by LVNC can likely alter myocardial stress.

We sought to determine the cardiac mechanics of patients with LVNC by finite element analysis. Specifically, the pressure-volume relationships, Starling's law and wall stress distribution were predicted for five patients retrospectively screened by ISMETT for LVNC. Cardiac mechanics of LVNC were compared to those of healthy patients as a control.

METHODS

Imaging and LV Segmentation

We retrospectively identified five patients with LVNC who underwent magnetic resonance imaging (MRI) from radiologic records of Mediterranean Institute for Transplantation and Advanced Specialized Therapies (ISMETT). This study was approved by our local ethical committee. Seven LV from healthy individuals matched for age with normal cardiac functionality were also included as controls. Patients underwent MRI as part of their care, and not for the purpose of our study. A series of long- and short-axis images of the heart were obtained performing MR imaging synchronized to the R wave of the electrocardiogram signal. Short -axis slices were taken sequentially every 6 mm until complete scanning of heart chambers.

From MRI, the two-layered structure of LVNC was modeled using two distinct approaches:

1. Compacted thin structure reconstructed from contour lines of the epicardium and the interface between noncompacted and compacted layers;
2. Noncompacted fibers modeled by Voronoi tessellation technique (Feng and Xiaolong 2016);

From MRI, the compacted thin structure was reconstructed from contour lines of MRI scans of the epicardium and the interface between noncompacted and compacted layers using contour lines in the vascular modeling toolkit VMTK (http://www.vmtk.org). Specifically, LV geometries were reconstructed at end-diastole (ED) and end-systole (ES), which are defined as the images with the maximum and minimum cross-sectional area, respectively. After segmentation process, the compacted thin structure was obtained by loft protrusion of segmented contour lines. In a different way, healthy controls were obtained by contour lines of the endocardial and epicardial MRI surfaces as done previously (Scardulla et al. 2015, 2016) (Rinaudo et al. 2014; Pasta, Gentile, et al. 2017) (Rinaudo et al. 2015; Gallo et al. 2018). For noncompacted structure, porosity of trabecular structure was quantified at apical, mid and basal LV regions using masks in the VMTK software. Specifically, a mask representative of the trabecular structure was reconstructed to compute the volume of the noncompacted structure. Similarly, a second mask was generated to segment the black voids within trabecular fibers to quantify the fraction of the volume of voids. The porosity was therefore computed as the fraction of the volume of voids over the total noncompaction volume. The Voronoi tessellation is a specific decomposition of a metric space based on a given set of random point. It subdivides a 3D space into polyhedra by connecting the bisecting lines or planes that are between pairs of points. By varying the density of the initial random points and the size of the tubes, we were able to obtain an isotropic 3D Voronoi-based geometry with a porosity equal to that measured for each patient using mask in VMTK. When the pore space is generated by assigning radii to the edges of the 3D Voronoi polyhedra cells, the resulted geometry is essentially a set of randomly inter-connected tubes representing the trabecular structure of noncompacted myocardial fibers. We applied the Voronoi tessellation technique using tools and commands implemented in the Grasshopper application of the computer-aided-design software Rhinoceros (v.5, Robert McNeel & Associates). The compacted and non-compacted structures were fixed by tie contact condition to generate the final shape of LVNC model (Figure 1).

Computational modelling

The space of compacted structure was meshed with 8-node brick elements to generate a volumetric mesh in ABAQUS/Explicit FE code (v.2018, Dassault Systemes). Using convergence analysis as previously reported (Scardulla et al. 2015), the element mesh ranged between 3945 and 5210 elements (type: C3D8), with four-element refinement along the myocardial thickness. Cardiac myofiber angles at the epicardium and endocardium were assigned to be -60 degrees and 60 degrees along the contour of LV wall, respectively (counterclockwise positive when viewed from the epicardium, see Figure 2). A linear variation of the myofiber angle was assumed from the epicardium to the endocardium throughout the LV wall. This was done by assigning local myofiber orientation to each element of the LVNC model using the ABAQUS graphical user interface. Differently, the complex shapes of trabecular structure obtained by Voronoi tessellation was meshed with tetrahedral elements.

Nearly incompressible, transversely isotropic, hyperelastic constitutive laws for passive and active myocardium developed by Guccione et al (Guccione et al. 2001) was implemented in ABAQUS/Explicit using a VUMAT subroutine. Energy was monitored to ensure the ratio of kinetic energy to internal energy remained less than 10%. Myocardial material parameters were estimated comparing MRI measured and computationally derived LV and RV volumes at ED and ES, respectively. Manual iteration was used rather than formal optimization. This procedure has therefore led to different material properties of the compacted myocardium versus the noncompacted fibers. Active contraction was neglected for noncompacted fibers given their lack of shortening capability (Bellavia et al. 2010; Fratini and Pasta 2010; van Dalen et al. 2011; Cutri et al. 2015; Pasta, Agnese, et al. 2017; Scardulla et al. 2017). Thus, a cylindrical coordinate system centered with the LV wall was used to provide the material orientation for the noncompacted fibers as shown by Figure 2. The ED solution was obtained by initially inflating

ventricular chambers to the intracavitary ED pressure to characterize the myocardial stiffness parameter. Thus, ES solution was achieved by setting the systolic intracavitary pressure and thus adding the active systolic contraction. For the compacted myocardial structure, the active contraction was modeled using a suitable scalar field (i.e., a fictitious temperature field in a thermal–mechanical analog approach) where the material parameters were increased during the systolic phase according to the force profile developed by cardiomyocytes as described by Cutri and collaborators (Cutri et al. 2015). This thermal–mechanical analog approach results in time-dependence material parameters, thereby modulating fiber-shortening of ventricular contraction. Although microscopic phenomena are neglected, this simplified approach reduces the model complexity and thus the computational cost. Both ED and ES solutions were obtained with intracavitary pressures of P_{ED}=22.5mmHg and P_{ES}=100mmHg.

For each simulation, ED and ES chamber volumes were used with corresponding P_{ED} and P_{ES} to plot ED and ES pressure-volume relationships (EDPVR and ESPVR, respectively). Both stroke volume SV/P_{ED} and SV/V_{ED} relationships were also determined.

RESULTS

Patients with LVNC had age of 44.3±22.8 yrs, body surface area of 2.0±0.2 m2, and ejection fraction (EF) of 52.5±3.5%, cardiac output (CO) of 5.4±1.9 l/min, ES volume V_{ES}=74.3±6.1 ml, ED volume V_{ED}=146.7±33.1 ml. Hypertrophy was observed for LVNC (e.g., 8.5±2.7 mm for LVNC and 5.2±1.5 mm for healthy LV at septum). The predominant localization of the porosity was at apex (44.7%) as compared to basal region (35.3%) of LVNCs. Table 1 summarizes clinical data of patients with LVNC and healthy control patients.

Patients with LVNC had a rightward shift of both ES and ED pressure-volume relationships as compared to those of healthy patients (Figure 3). The rightward shift of the ES pressure-volume

relationship suggests a decrease in the compliance of patients with LVNC and highest LV volume when compared to that of controls at the same intracavitary blood pressure. This change in the myocardial elastance was less pronounced for ED pressure-volume showing less rightward shift and thus a minimal increase in the LV volume during diastole as compared to that of controls. Indeed, ES elastance was lower than that of healthy patients (i.e., 2.5mmHg/ml for LVNC and 9.5mmHg/ml for healthy patients), suggesting reduced systolic function for the patient with LVNC. Stroke volume (SV) was reduced for LVNC when compared to those of healthy patients at the same level of diastolic pressure. For LVNC, the Starling's curve (i.e. SV/P_{ED}) lied on the right compared to that of normal hearts (Figure 4A). As indicated by SV/V_{ED}, LVNC requires higher values of V_{ED} than control hearts to pump the same amount of SV (Figure 4B).

Noncompacted fibers had significantly higher myocardial wall stresses than those of healthy LV (i.e., 91 kPa for LVNC and 62 kPa for healthy LV at ES, $p<.05$), with magnitude according to fiber porosity (Figure 4). Distribution of myocardial fiber stress at ED for two cases with LVNC demonstrates that the noncompacted structure has higher myocardial stress than the compacted heart structure (Figure 6). The differences in trabeculation mostly influenced the resulting wall stress. Furthermore, LV ES rotation was reduced upon 60% for the patient with LVNC as compared to that of healthy controls (Figure 7).

DISCUSSION

This study was undertaken to demonstrate that patient-specific computational analysis can be adopted to evaluate the severity of patients with LVNC by a noninvasive quantification of ventricular diseases and altered wall stress. Findings illustrated impaired cardiac mechanics for LVNC, making it possible that the lack of fiber shortening induced by the noncompacted structure can lead to LV volume reduction during isovolumic contraction. At same level of

diastolic pressure, SV was reduced for LVNC when compared to that of healthy LV. The noncompacted myocardial structure of LVCN is the main determinant of reduced pump performance and high myocardial wall stress. The high the wall stress is, the high is the risk of adverse ventricular remodeling. These findings suggest reduced systolic function for patients with LVNC with respect to healthy controls. Computational modeling may allow personalized approach to improve the way we diagnose and treat cardiac disorders

~~. Simulations were carried out to assess cardiac mechanics of cardiomyopathy (Quarterman et al. 2002; Scardulla et al. 2016), pericardial effusion (Scardulla et al. 2015), left ventricular assist device (Sack et al. 2018; Scardulla, Agnese, et al. 2018), right heart failure induced by pulmonary hypertension (Scardulla, Bellavia, et al. 2018) using models of left ventricular chamber alone or including both left and right heart ventricular chambers. For instance, Wenk et al. (Jhun et al. 2010) evinced that residual stress produced by ventricular volume reduction surgery has a little effect on the LV function and cardiac mechanics. Another study suggests that surgical anterior ventricular restoration reduces myofiber stress in the akinetic infarct at the expense of a reduction in the Starling relationship (Jhun et al. 2010). Simulations also demonstrated that aneurysm implication decreases fiber stress without depressing stroke volume (Guccione et al. 2001; Walker et al. 2005). Carrick et al. (Carrick et al. 2012) highlighted that Coapsys procedure decreases myofiber stress at ED and ES, and that the improvement in myofiber stress may contribute to the long-term effect of Coapsys on LV remodeling. With regards to cardiomyopathy, Zhog et al. (Zhong et al. 2009) investigated LV remodeling in ischemic cardiomyopathy using FE modeling. They suggested that LV remodeling in ischemic cardiomyopathy is a multistep process, which determines loss of contractile function followed by acute dilatation of the infarction area, increase of LV volume, lengthening of the LV perimeter, and blunting of the normal curvature. Wall stress were found increased in each region of LV wall and has been shown to be a measure of the afterload following infarction.~~ Computational

modeling has been widely used to study cardiac diseases, but the effect the effect of the irregular structure of the LV trabeculae on the cardiac mechanics is poorly understood. Using a computational modeling, Sacco and collaborators (Sacco et al. 2018)demonstrated that the LV trabeculae structure alters the cardiac hemodynamics by increasing the intraventricular pressure drop and disrupting the dominant single vortex when compared to that of a model with a smooth endocardial surface. Similarly, Serrani et al (Serrani et al. 2013) found that the presence of trabecular mass contributes to the ventricular filling, allowing a higher ventricular stroke volume. To our knowledge, however, our study is the first investigation of the cardiac mechanics of LVNC. We found that LVNC-related wall stresses are higher than that of healthy subjects, suggesting adverse cardiac remodeling.

Another key advantage of computational modeling is that it has an extensive capability in predicting ventricular pump function, which is impossible to do using conventional echocardiography. In this study, we observed that passive filling is impaired in LVNC as compared to that of healthy controls. Once more, it should be noted that the computationally-derived SV/P_{ED} relationship could be a better metric of pump performance as compared to commonly used EF, which directly depends on LV volume and hence susceptible to misinterpretation in the setting of noncompacted left chamber. We also found that LVNC have reduced rotation, which was found as a prognostic determinant of adverse clinical outcome from speckle-tracking echocardiography (Bellavia et al. 2010; van Dalen et al. 2011).

Although this computational approach highlighted several aspects of LVNC-related cardiac mechanics, there are several limitations in the computational modeling approach. It should be also considered that technical expertise is needed to carry out such computational approach so that clinical application is still far away. However, current research based on machine learning can enhance the application of computational modeling in cardiac diseases (Bellavia et al. 2019;

Leiner et al. 2019). Another significant limitation is that healthy controls were not matched for wall thickness of patients with LVNC. This likely affect myocardial stress which is given by the ratio of the pressure exerted on the LV endocardial surface. To quantify the effect of wall thickness on the resulting stress distribution, virtual models based on the LV mass or thickness of patients with LVNC patients could be adopted to generate a virtual cohort of controls. Then new simulations could be performed to compare stress values between matched groups. The MRI scan had a resolution in the z-axis of 6 mm, and this has likely hidden several geometrical features of the noncompacted myocardial structure. Other limits include calculation of regional myocardial material properties. There is also a limited number of patients with LVNC, with not any invasive analysis of cardiac function by catheterization. Therefore, the here presented pressure-volume loops need validation with catheter-based measurements but this was not possible for our patients with LVNC. In patients who routinely undergo catheterization, we demonstrated a good agreement between computationally-predicted and catheter-based hemodynamic measurements [12]. Although this supports in part the results here presented, a validation with clinical hemodynamic measurements is advocated.

CONCLUSION

In this study, we demonstrated the capability of computational modeling to predict the severity of patients with LVNC by noninvasively predicting myocardial stress and pump performance. Patients with LVNC were characterized by reduced systolic function and impaired cardiac mechanics with lack of fiber shortening induced by noncompacted layer. The difference in pump performance between LVCN and healthy LV geometries are likely responsible for the high myocardial wall stress, which could be a responsible for adverse ventricular remodeling. We foresee that patient-specific computational modeling may even form the basis for clinical decision-making process related to the intervention of cardiac diseases.

REFERENCES

Bellavia D, Iacovoni A, Agnese V, Falletta C, Coronnello C, Pasta S, Novo G, di Gesaro G, Senni M, Maalouf J et al. 2019. Usefulness of regional right ventricular and right atrial strain for prediction of early and late right ventricular failure following a left ventricular assist device implant: A machine learning approach. The International journal of artificial organs.391398819884941.

Bellavia D, Michelena HI, Martinez M, Pellikka PA, Bruce CJ, Connolly HM, Villarraga HR, Veress G, Oh JK, Miller FA. 2010. Speckle myocardial imaging modalities for early detection of myocardial impairment in isolated left ventricular non-compaction [Research Support, Non-U.S. Gov't]. Heart. 96(6):440-447. eng.

Carrick R, Ge L, Lee LC, Zhang Z, Mishra R, Axel L, Guccione JM, Grossi EA, Ratcliffe MB. 2012. Patient-specific finite element-based analysis of ventricular myofiber stress after Coapsys: importance of residual stress. Ann Thorac Surg. 93(6):1964-1971. eng.

Cutri E, Serrani M, Bagnoli P, Fumero R, Costantino ML. 2015. The cardiac torsion as a sensitive index of heart pathology: A model study. J Mech Behav Biomed Mater. 55:104-119.

Feng X, Xiaolong Y. 2016. Geometry models of porous media based on Voronoi tessellations and their porosity–permeability relations. Computers & Mathematics with Applications. 72(2):328-348.

Fratini L, Pasta S. 2010. Residual Stresses in Friction Stir Welded Parts of Complex Geometry. International Journal of Advanced Manufacturing Technology. 59(5-8):547-557.

Gallo A, Agnese V, Coronnello C, Raffa GM, Bellavia D, Conaldi PG, Pilato M, Pasta S. 2018. On the prospect of serum exosomal miRNA profiling and protein biomarkers for the diagnosis of ascending aortic dilatation in patients with bicuspid and tricuspid aortic valve. Int J Cardiol. 273:230-236.

Guccione JM, Moonly SM, Moustakidis P, Costa KD, Moulton MJ, Ratcliffe MB, Pasque MK. 2001. Mechanism underlying mechanical dysfunction in the border zone of left ventricular aneurysm: A finite element model study. Annals of Thoracic Surgery. 71(2):654-662. English.

Ichida F. 2009. Left ventricular noncompaction. Circ J. 73(1):19-26. eng.

Jenni R, Oechslin E, Schneider J, Attenhofer Jost C, Kaufmann PA. 2001. Echocardiographic and pathoanatomical characteristics of isolated left ventricular non-compaction: a step towards classification as a distinct cardiomyopathy. Heart. 86(6):666-671. eng.

Jhun CS, Wenk JF, Zhang Z, Wall ST, Sun K, Sabbah HN, Ratcliffe MB, Guccione JM. 2010. Effect of adjustable passive constraint on the failing left ventricle: a finite-element model study. Ann Thorac Surg. 89(1):132-137. eng.

Lee LC, Genet M, Dang AB, Ge L, Guccione JM, Ratcliffe MB. 2014. Applications of computational modeling in cardiac surgery [Research Support, N.I.H., Extramural Research Support, Non-U.S. Gov't]. Journal of cardiac surgery. 29(3):293-302. eng.

Leiner T, Rueckert D, Suinesiaputra A, Baessler B, Nezafat R, Isgum I, Young AA. 2019. Machine learning in cardiovascular magnetic resonance: basic concepts and applications. Journal of cardiovascular magnetic resonance : official journal of the Society for Cardiovascular Magnetic Resonance. 21(1):61.

Pasta S, Agnese V, Di Giuseppe M, Gentile G, Raffa GM, Bellavia D, Pilato M. 2017. In Vivo Strain Analysis of Dilated Ascending Thoracic Aorta by ECG-Gated CT Angiographic Imaging. Ann Biomed Eng. 45(12):2911-2920.

Pasta S, Gentile G, Raffa GM, Bellavia D, Chiarello G, Liotta R, Luca A, Scardulla C, Pilato M. 2017. In Silico Shear and Intramural Stresses are Linked to Aortic Valve Morphology in Dilated Ascending Aorta. Eur J Vasc Endovasc Surg. S1078-5884(17):30331-30333.

Quarterman RL, Moonly S, Wallace AW, Guccione J, Ratcliffe MB. 2002. A finite element model of left ventricular cellular transplantation in dilated cardiomyopathy. ASAIO J. 48(5):508-513. eng.

Ratcliffe MB, Hong J, Salahieh A, Ruch S, Wallace AW. 1998. The effect of ventricular volume reduction surgery in the dilated, poorly contractile left ventricle: A simple finite element analysis. J Thorac Cardiov Sur. 116(4):566-577. English.

Rinaudo A, D'Ancona G, Lee JJ, Pilato G, Amaducci A, Baglini R, Folli C, Pilato M, Pasta S. 2014. Predicting Outcome of Aortic Dissection with Patent False Lumen by Computational Flow Analysis. Cardiovasc Eng Technol. 5(2):176-188.

Rinaudo A, Raffa GM, Scardulla F, Pilato M, Scardulla C, Pasta S. 2015. Biomechanical implications of excessive endograft protrusion into the aortic arch after thoracic endovascular repair. Computers in biology and medicine. 66:235-241. English.

Sacco F, Paun B, Lehmkuhl O, Iles TL, Iaizzo PA, Houzeaux G, Vazquez M, Butakoff C, Aguado-Sierra J. 2018. Left Ventricular Trabeculations Decrease the Wall Shear Stress and Increase the Intra-Ventricular Pressure Drop in CFD Simulations. Frontiers in physiology. 9:458.

Sack KL, Dabiri Y, Franz T, Solomon SD, Burkhoff D, Guccione JM. 2018. Investigating the Role of Interventricular Interdependence in Development of Right Heart Dysfunction During LVAD Support: A Patient-Specific Methods-Based Approach. Frontiers in physiology. 9:520.

Sarma RJ, Chana A, Elkayam U. 2010. Left ventricular noncompaction [Review]. Prog Cardiovasc Dis. 52(4):264-273. eng.

Scardulla F, Agnese V, Romano G, Di Gesaro G, Sciacca S, Bellavia D, Clemenza F, Pilato M, Pasta S. 2018. Modeling Right Ventricle Failure After Continuous Flow Left Ventricular Assist Device: A Biventricular Finite-Element and Lumped-Parameter Analysis. Cardiovascular engineering and technology. 9(3):427-437.

Scardulla F, Bellavia D, Vitulo P, Romano G, Mina C, Gentile G, Clemenza F, Pasta S. 2018. Biomechanical Determinants of Right Ventricular Failure in Pulmonary Hypertension. ASAIO J. 64(4):557-564.

Scardulla F, Pasta S, D'Acquisto L, Sciacca S, Agnese V, Vergara C, Quarteroni A, Clemenza F, Bellavia D, Pilato M. 2017. Shear stress alterations in the celiac trunk of patients with a continuous-flow left ventricular assist device as shown by in-silico and in-vitro flow analyses. The Journal of heart and lung transplantation : the official publication of the International Society for Heart Transplantation. 36(8):906-913.

Scardulla F, Rinaudo A, Pasta S, Scardulla C. 2015. Mechanics of pericardial effusion: a simulation study. Proc Inst Mech Eng H. 229(3):205-214.

Scardulla F, Rinaudo A, Pasta S, Scardulla C. 2016. Evaluation of ventricular wall stress and cardiac function in patients with dilated cardiomyopathy. Proc Inst Mech Eng H. 230(1):71-74.

The influence of cardiac trabeculae on ventricular mechanics. Computing in Cardiology 2013; 22-25 Sept. 2013 2013; Zaragoza, Spain

van Dalen BM, Caliskan K, Soliman OI, Kauer F, van der Zwaan HB, Vletter WB, van Vark LC, Ten Cate FJ, Geleijnse ML. 2011. Diagnostic value of rigid body rotation in noncompaction cardiomyopathy. J Am Soc Echocardiogr. 24(5):548-555. eng.

Walker JC, Ratcliffe MB, Zhang P, Wallace AW, Fata B, Hsu EW, Saloner D, Guccione JM. 2005. MRI-based finite-element analysis of left ventricular aneurysm. Am J Physiol-Heart C. 289(2):H692-H700. English.

Zhong L, Su Y, Yeo SY, Tan RS, Ghista DN, Kassab G. 2009. Left ventricular regional wall curvedness and wall stress in patients with ischemic dilated cardiomyopathy. Am J Physiol-Heart C. 296(3):H573-H584. English.

Table 1. Baseline characteristics of patient population; *denotes significant difference after Mann-Whitney U test ($p<.05$) with the healthy control group;

	Healthy (n=7)	**LVNC** (n=5)
Characteristics		
***Age**, years*	41±16	44.3±22.8
***Male,** %*	57 (4)	80 (4)
***BSA,** m^2*	1.8±0.2	2.0±0.2
***HR,** bpm*	70±18	75±12
Imaging		
***EF,** %*	60.3±4.2	52.5±3.5 *
***CO,** l/min*	5.1±2.4	5.4±1.9
***V_{ED},** ml*	124.1±18.4	146.7±33.1
***V_{ES},** ml*	50.4±8.1	74.3±6.1 *

Figure Legends

Figure 1: (A) Sketch of a LVNC; (B) MRI image of LVNC at mid short-axis of left chamber; (C) render of fiber trabeculations modeled generated by Voronoi tesselletion; (D) two layered structure of LVNC showing compacted myocardium (left model) and noncompacted fibers (right model)

Figure 2: Mesh of the LVNC model showing the myofiber direction and material orientation

Figure 3: Pressure–volume relationships for normal hearts (■) and patients with LVNC (○)

Figure 4: (A) SV/P_{ED} (i.e. Starling's law) and (C) SV/V_{ED} profiles for normal hearts (■) and patients with LVNC (○)

Figure 5: Maxima of myocardial wall stress at ES (■) and ED (□) for normal hearts and patients with LVNC; * significantly different from LVNC ES stress, $p<.05$

Figure 6: Distribution of myocardial fiber stress at ED for two cases with LVNC; right models shows a cross-section of LVNC

Figure 7: ES LV rotation calculated as the LV rotation angle at apical short-axis plane in the same point

Fig1

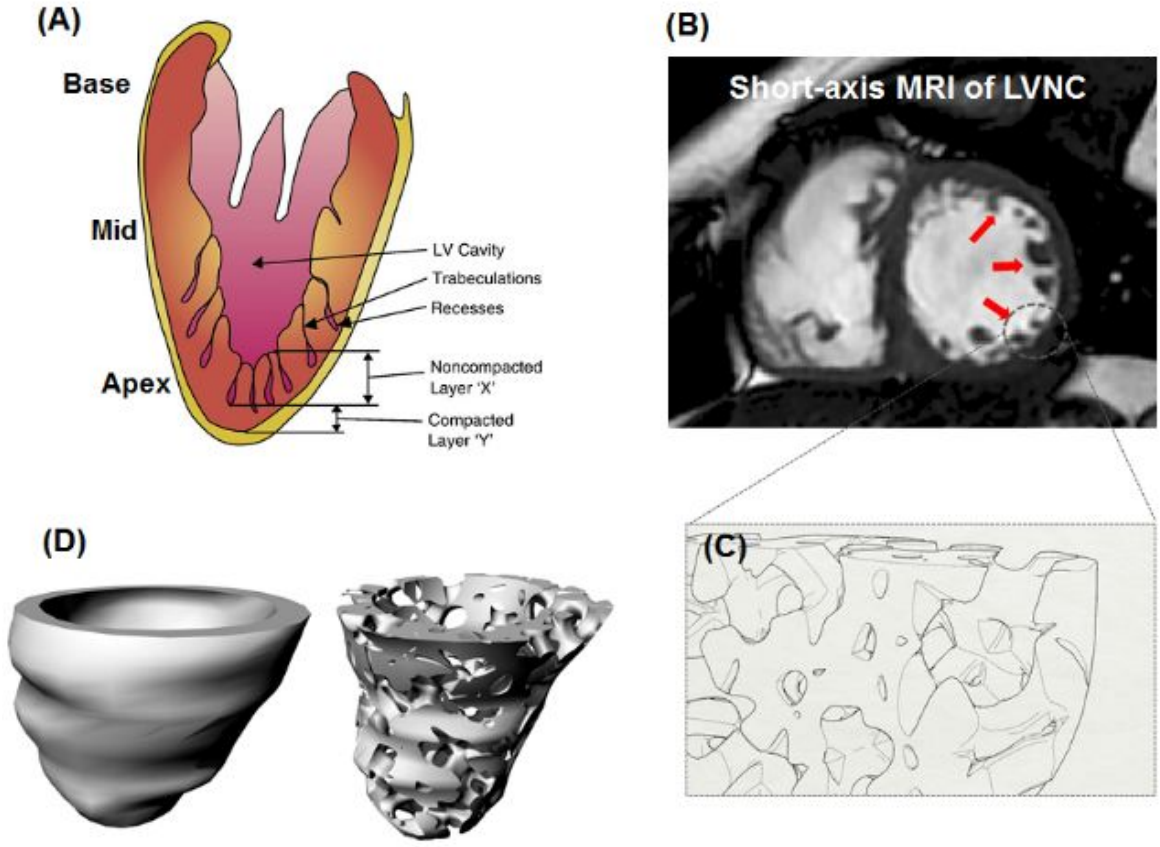

Fig2

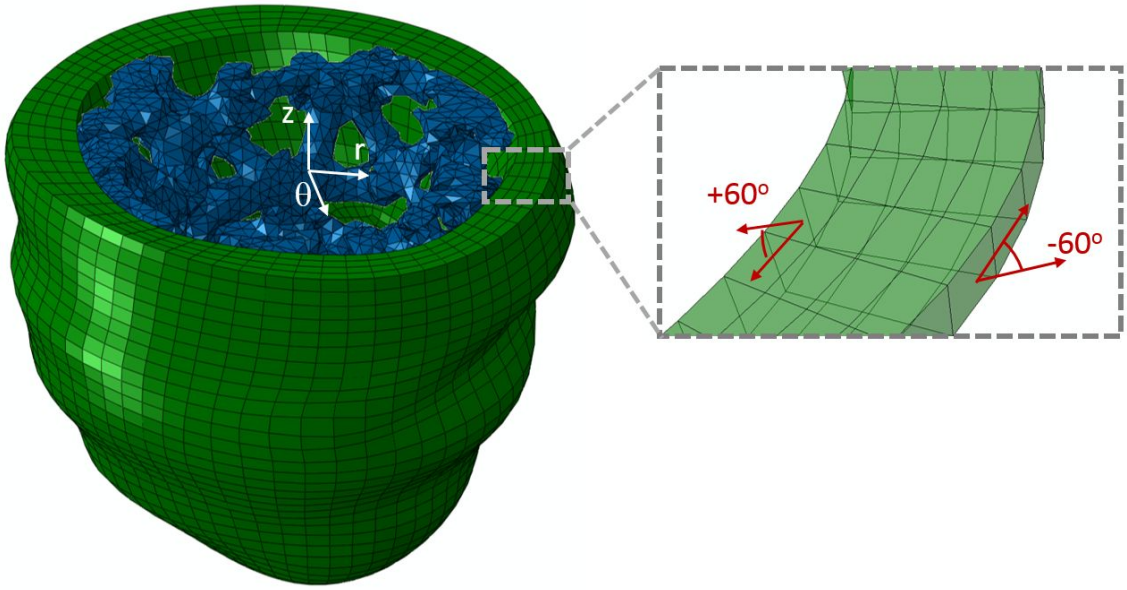

Fig3

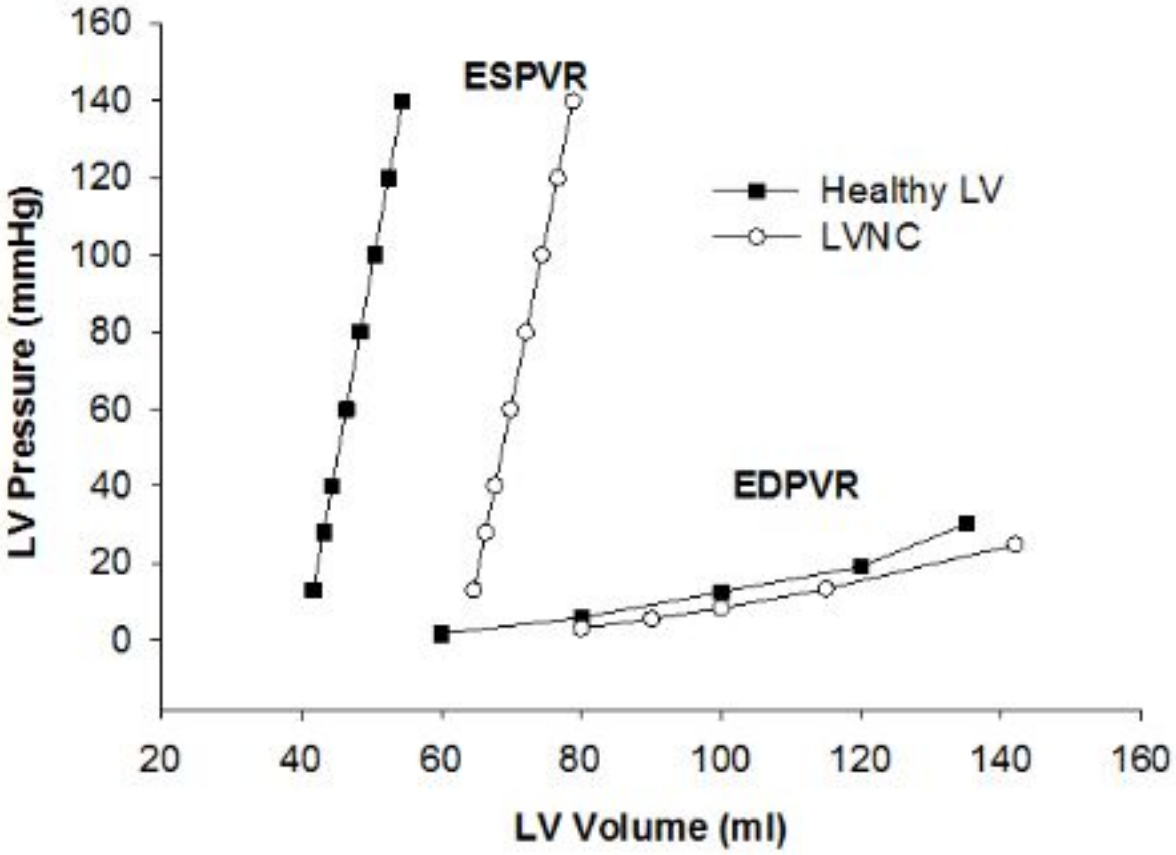

Fig4

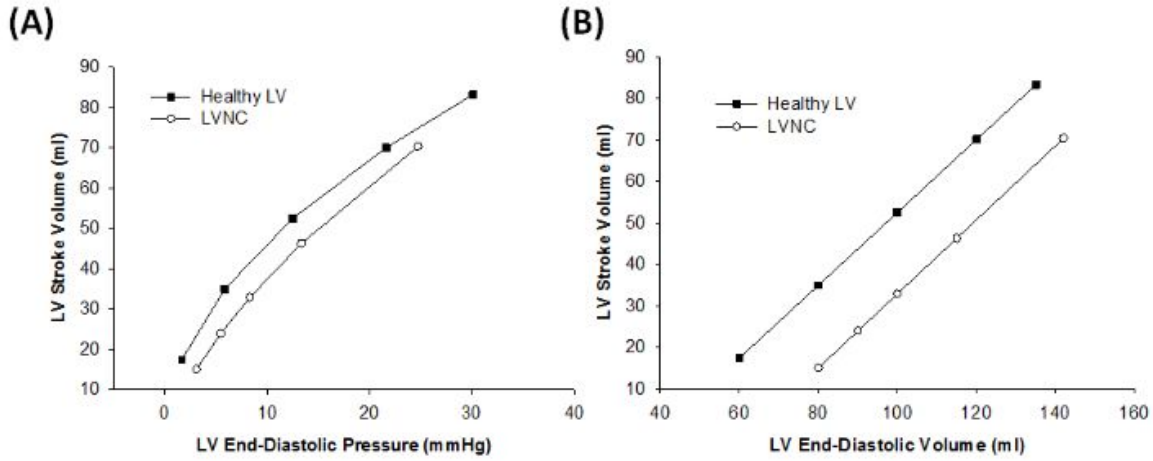

Fig5

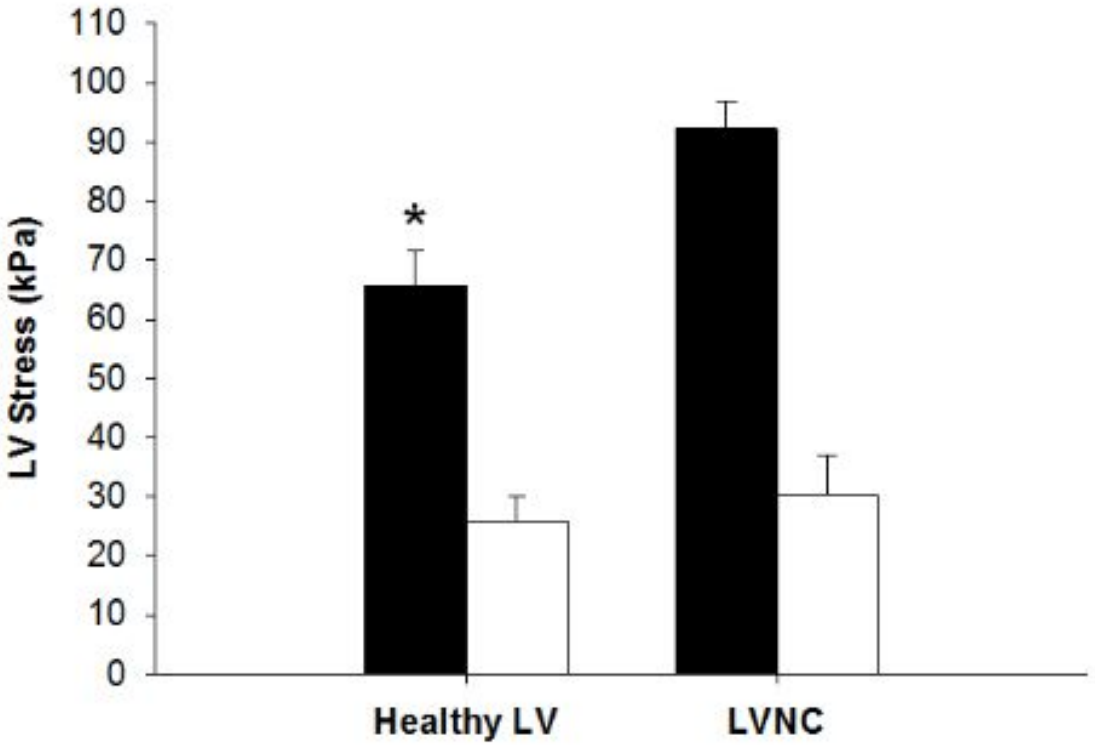

Fig6

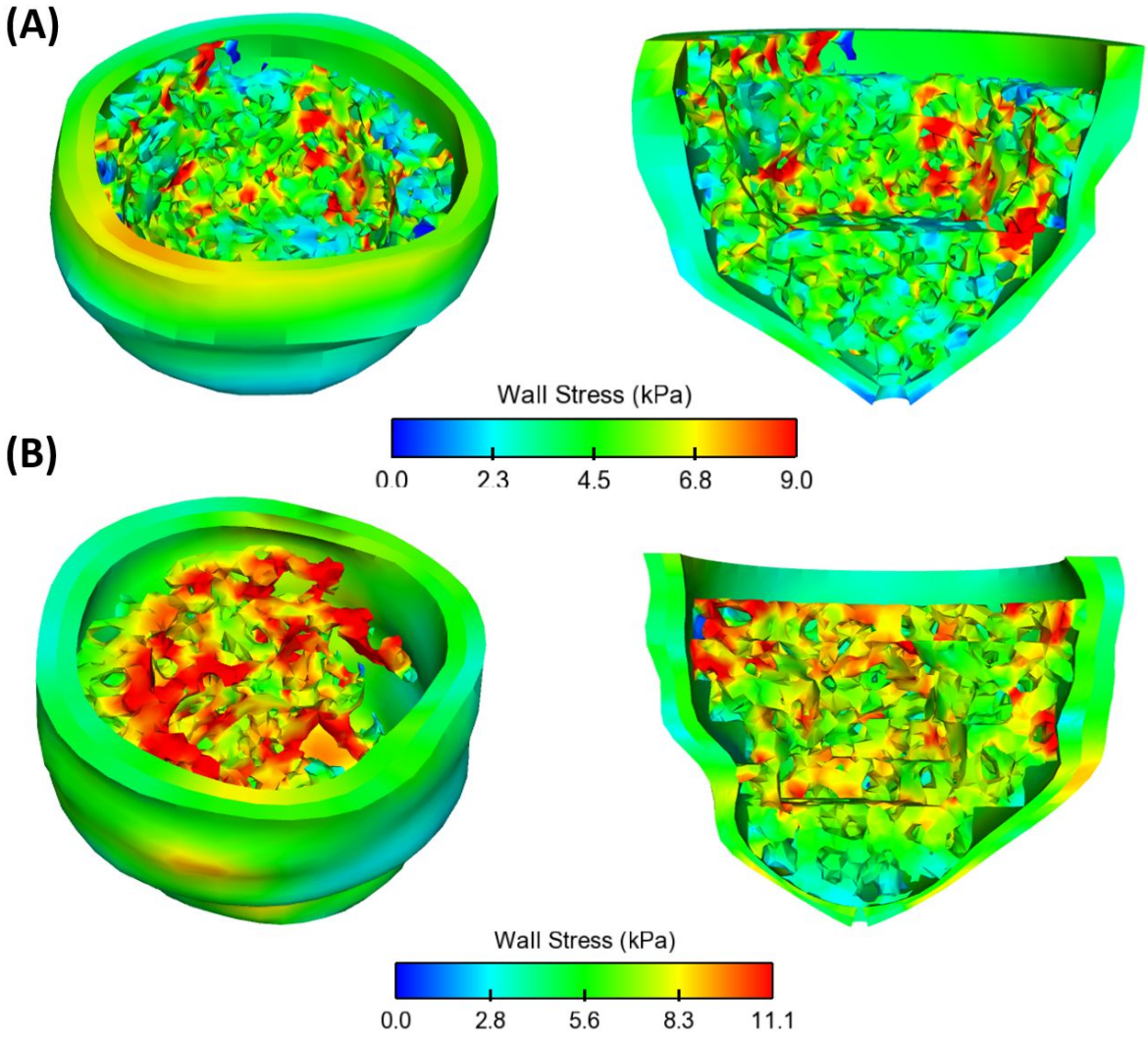

Fig7